Journal of Applied Fluid Mechanics, Vol. 12, No. 5, pp. 1449-1461, 2019.
Available online at www.jafmonline.net, ISSN 1735-3572, EISSN 1735-3645.
DOI: 10.29252/jafm.12.05.29704

Study on the Accuracy of RANS Modelling of the Turbulent Flow Developed in a Kaplan Turbine Operated at BEP. Part 1 - Velocity Field

R. G. Iovănel[1, 2†], D. M. Bucur[1] and M. J. Cervantes[2]

[1] *University Politehnica of Bucharest, 060042, Romania*
[2] *Luleå University of Technology, 971 87, Sweden*

†*Corresponding Author Email: raluca.iovanel@gmail.com*

(Received October 8, 2018; accepted January 12, 2019)

ABSTRACT

This paper investigates the accuracy of Reynolds-averaged Navier-Stokes (RANS) turbulence modelling applied to complex industrial applications. In the context of the increasing instability of the energy market, hydropower plants are frequently working at off-design parameters. Such operation conditions have a strong impact on the efficiency and life span of hydraulic turbines. Therefore, research is currently focused on improving the design and increasing the operating range of the turbines. Numerical simulations represent an accessible and cost efficient alternative to model testing. The presented test case is the Porjus U9 Kaplan turbine model operated at best efficiency point (BEP). Both steady and unsteady numerical simulations are carried out using different turbulence models: k-epsilon, RNG k-epsilon and k-omega Shear Stress Transport (SST). The curvature correction method applied to the SST turbulence model is also evaluated showing nearly no sensitivity to the different values of the production correction coefficient C_{scale}. The simulations are validated against measurements performed in the turbine runner and draft tube. The numerical results are in good agreement with the experimental time-dependent velocity profiles. The advantages and limitations of RANS modelling are discussed. The most accurate results were provided by the simulations using the k-epsilon and the SST-CC turbulence models but very small differences were obtained between the different tested models. The precision of the numerical simulations decreased towards the outlet of the computational domain. In a companion paper, the pressure profiles obtained numerically are investigated and compared to experimental data.

Keywords: Numerical simulation; Turbulence modelling; Hydropower; Kaplan turbine; Experimental validation.

NOMENCLATURE

C_{scale}	production correction coefficient	V^*	dimensionless tangential velocity
D	runner diameter	u', v', w'	fluctuating velocity components
k	turbulent kinetic energy	y^+	dimensionless wall distance
R	runner radius		
R^*	dimensionless runner radius		
U^*	dimensionless axial velocity	ε	turbulent dissipation

1. INTRODUCTION

The sustainable use of fossil fuels and the continuous development of electricity production from renewable energy sources are highly encouraged nowadays, but at the cost of energy grid stability. By managing long term storage capacities and providing the only existing large scale storage solutions, hydropower is able to back-up the integration of renewable energy and contribute to the security and continuity of energy supply (Hirth, 2016; Belman-Flores *et al.*, 2016). The economic and environmental benefits of hydropower justify the further development of the existing technology and the exploitation of the remaining potential in a cost-efficient and affordable manner. Of the same importance are the rehabilitation of current hydraulic schemes and the optimization of the new

turbines design, taking into account the recurrence of transient operating conditions (Rahi and Chandel, 2015).

Hydroelectric power plants equipped with Kaplan turbines provide one of the solutions to the grid balancing problem. Kaplan turbines are double-regulated axial machines used on sites with low net heads and relatively high flow rates. The blade angles of the guide vanes and runner blades can be adjusted separately, thus providing good efficiency across a wide flow range, and a flat efficiency curve (Lipej and Poloni, 2000). However, the flow inside Kaplan turbines is particularly challenging to predict due to the complex geometry. The construction with rotating blades determines the tip edges to move near the shroud wall and the rotating hub, therefore secondary flows occur and the flow behavior is difficult to capture (Roussopoulos and Monkewitz, 2000). Another specific feature of Kaplan turbines is the rotor-stator interaction that is known to induce pressure fluctuations on the runner blades (Amiri *et al.*, 2015). As opposed to Francis turbines that have a small gap between the rotor and the stator, Kaplan turbines have a rather large vaneless space. The flow in this region becomes more complex given the dissipation of the wakes coming from the stator blades and the rotation of the flow. The draft tube also has an important role in the performance of Kaplan turbines, having a strong influence over the efficiency of low head turbines in general. The analysis of the flow in the draft tube is both challenging and time consuming due to the flow features (Abbas and Kumar, 2015).

The most important instruments in the design and the modernization processes of hydraulic turbines are model testing and numerical simulations. Given the costs, the duration and the limited amount of information that experimental investigations provide, such studies alone cannot support the entire rehabilitation process (Wu *et al.*, 2006; Prasad, 2012). Since the early 80's, Computational Fluid Dynamics techniques (CFD) are more frequently used by the manufacturers at the design stage. Numerical simulations allow the testing of several design alternatives in a shorter time, compared to model testing. Nevertheless, the numerical tools available are still limited and need improvements (Keck and Sick, 2008).

The Reynolds-averaged Navier-Stokes (RANS) turbulence models are two-equation eddy-viscosity models (Alfonsi, 2009). These models are robust and are not computationally expensive. Therefore, they are a common choice for both steady and unsteady simulations. It is often mentioned (Arolla and Durbin, 2014; Elliot *et al.*, 2012) that eddy-viscosity turbulence models are not accurately capturing the effects of the streamline curvature and system rotation due to the assumption of isotropy of the turbulent viscosity, i.e., the ratio between Reynolds stress and mean rate of deformations is considered constant in all three directions. The Reynolds Stress Models (RSM), on the other hand, do not use the eddy-viscosity model. The Reynolds stresses are directly computed based on the exact Reynolds stress transport equation and the effects of the different components of the Reynolds stress tensor are captured. However, it can become challenging to model the flow in hydraulic turbines since RSM are computationally expensive and encounter difficulties in achieving convergence.

In order to account for the disadvantages of the eddy-viscosity turbulence models, Spalart and Shur (1997) introduced a rotation and curvature correction that was described by the authors as "an empirical alteration of eddy-viscosity models". In their study, the authors presented the application of this idea to the Spalart-Allmaras one-equation model. Smirnov and Menter (2009) have adapted this correction to the Shear Stress Transport (SST) turbulence model with minor modifications. The empirical function proposed in Spalart and Shur (1997) was used as a multiplier of the production term. A scaling coefficient C_{scale} was introduced in Ansys CFD to allow the user to control the effect of the curvature correction. The curvature corrected SST model was found to be accurate when predicting complex three dimensional rotating flows. The SST-CC turbulence model was recently used by Javadi *et al.* (2015) in the investigation of the swirling flow in a Francis turbine draft tube and a swirl generator. It was shown that the recirculation region was predicted accurately but the mean velocity prediction showed no major improvement. Also, as stated by the authors, the tuning of the model did not improve the quality of the results.

Hydraulic turbines have been investigated using CFD modelling and several reference studies are available for academic research. Advanced simulations have been performed for Francis turbines. The Francis-99 test case provides access to the entire three-dimensional geometry of a high head Francis model, hexahedral mesh and experimental data. Comparisons between numerical simulations and experimental results have been discussed in a series of workshops (Trivedi *et al.*, 2016a). BulbT, a similar project, provided flow measurements in a bulb turbine model. Numerical studies were carried out investigating the hub and tip clearances and their influence on the turbine performance (Vu *et al.* 2014). However, concerning Kaplan turbines, only a few experimental studies are currently available for comparison to CFD simulations with the exception of the Turbine-99 test case (Cervantes and Engström, 2005, Cervantes *et al.*, 2010).

In the current paper, the Porjus U9 Kaplan turbine model is investigated numerically. There are three different approaches that may be used when modelling the flow in hydraulic turbines, (Trivedi *et al.*, 2016b): the modelling of a complete turbine, the modelling of the runner and distributor or draft tube and the single component modelling.

Previously, Mulu *et al.* (2011) studied the effects of the inlet boundary conditions over the accuracy of Kaplan draft tube simulations in the Porjus U9 model. Using Ansys CFX, a simulation was run for the single draft tube domain, with the inlet surface right below the runner cone. Experimentally

obtained axial and tangential velocity profiles were defined as inlet boundary condition and the radial velocity was neglected in their simulation. The second approach was a Stage simulation. The computational flow domains used for the Stage simulation were the flow channels corresponding to one guide vane, one runner blade and the draft tube. The mass flow rate was specified as inlet boundary condition. Different RANS turbulence models were tested: k-epsilon, RNG k-epsilon, SST, SSG Reynolds stress model and Baseline (BSL) k-omega model. The central vortex in the draft tube cone was not captured correctly by the two-equation models, whereas the RSM proved to be more accurate in predicting the flow below the runner cone. The Stage simulation showed no sensitivity to the different turbulence models, all of them predicting an early separation on the runner cone.

A more detailed numerical analysis of the same Kaplan turbine model was introduced by Mulu *et al.* (2015). The study presented a comparison between the unsteady simulation and the experimental values, this time including the full guide vane domain, entire runner and draft tube. The turbulence models considered were: k-epsilon, RNG k-epsilon and SST. The near hub flow was better modelled and the main draft tube flow characteristics were captured. However, all the turbulence models had problems predicting the high axial velocity that resulted from the blade-hub clearance. As a consequence, the flow was detached from the runner cone.

The aim of the present paper is to find the fastest and easiest way to accurately capture the flow throughout a Kaplan turbine. Steady-state and unsteady simulations of the flow in the Porjus U9 Kaplan turbine model under steady-state operation at BEP are compared. The Porjus U9 model has been experimentally investigated and a large amount of measurements are available starting from the inlet pipe down to the draft tube outlet (Amiri *et al.*, 2016a; Mulu and Cervantes, 2009; Mulu and Cervantes, 2011; Amiri *et al.*, 2016b). The numerical simulations are validated against velocity profiles measured in the runner blade channel, below the runner blades and in the draft tube cone and diffuser. Compared to the previous studies, the computational domain features a more accurate geometry including the scanned runner blade and the hub and tip clearances. The draft tube inlet surface is lowered below the runner cone, thus completely separating the runner rotating domain from the stationary draft tube. For each type of simulation, three turbulence models have been tested: k-epsilon, RNG k-epsilon and SST. The curvature corrected SST model was also employed, using the production correction coefficient at its standard value C_{scale} = 1 and 1.25. In a second paper, the numerical results are compared to pressure measurements investigating the pressure fluctuations on the runner blades and the sources of asymmetric hydraulic loads present in a Kaplan turbine runner during BEP operation.

2. TEST CASE

A detailed description of the test rig, the Porjus U9 Kaplan model and the experimental results can be found in (Amiri *et al.*, 2016a). Both the Porjus U9 Kaplan prototype and model (1:3.1 scale), consist of a spiral casing, 18 stay vanes, 20 guide vanes, 6 runner blades and the draft tube. The diameter of the model runner is D = 0.5 m. The operational net head is 7.5 m and the runner rotational speed is 696.3 rpm. The model specifications for the BEP are the guide vane angle of 26.5° and a corresponding volume flow rate of 0.69 m^3s^{-1}.

Amiri *et al.* (2016a) used a two-component Laser Doppler Anemometry (LDA) system to investigate the interblade flow in the Porjus U9 model during BEP and off-cam operating conditions. Axial and tangential velocity profiles were presented for the blade channel region and below the runner blades at the runner outlet (Fig. 1). The hub and shroud clearances leakage were found to be the main sources of velocity fluctuations and also the cause of some hydraulic losses in the runner. No tip vortex was captured by the measurements performed in the blade channels but both hub and tip vortices formed in the blade clearances were visible at the runner outlet.

The unsteady three dimensional turbulent flow developed in the draft tube was investigated by Mulu *et al.* (2009) using LDA at three different axial positions and four angular positions presented in Fig. 1. The first and second measurement sections were located right below the runner cone and in the middle of the draft tube cone. The last measurement section was located at the end of the cone, above the draft tube elbow (Fig. 1). Velocity profiles were measured perpendicular to the draft tube cone wall which had an angle of 6.1°. The axial and tangential velocity profiles measured at BEP were presented. The phase averaged mean velocity measurements together with the corresponding fluctuations were analyzed by Mulu and Cervantes (2011) and the effects of the runner blade wakes on the flow distribution in the draft tube cone were studied.

Amiri *et al.* (2016b) also investigated the flow condition in the Porjus U9 draft tube performing Particle Image Velocimetry (PIV) measurements in the draft tube diffuser, after the elbow. The measurements were performed at two different locations: downstream the draft tube bend and near the draft tube outlet. The velocity components were obtained for each of the two locations on a net formed by three horizontal planes and five vertical planes. At the upstream window the planes covered an area of 1270×375 mm (lateral and vertical); in the downstream window the covered area was 1270×485 mm (Fig. 1). On the horizontal planes the axial and lateral velocities were presented and the vertical measurement planes showed the axial and vertical velocities. The authors found that the velocity distributions inside the diffuser were influenced by the turbine operating point and the swirl at the runner outlet.

Table 1 Quality parameters of the mesh

Domain	Minimum angle [°]	Expansion factor	Aspect ratio
Guide vane	19.9	21	84
Runner	16.8	48	668
Draft tube	30.5	9	7635

3. NUMERICAL CASE

In the current study, two types of simulations were carried out using ANSYS CFX 16.2: steady-state simulations using Stage interfaces and unsteady simulations using Transient Rotor-Stator interfaces. A steady-state simulation employing the Frozen Rotor interface was used to provide the initial values, since it is computationally inexpensive and it is considered numerically robust.

Steady-state simulations are simulations which assume that the flow characteristics are independent of time. The steady conditions have been already reached before the beginning of the simulation; therefore real time information is not required. Unsteady simulations are generally used for time dependent operations with time dependent initial conditions, i.e., load variation, and need real time information at which the CFX Solver calculates the flow characteristics. However, there are also cases of transient behavior when even if flow conditions are not changing, a steady-state condition cannot be reached, e.g., rotating runner. Considering this, unsteady simulations are also performed, although the Porjus U9 is investigated under steady-state operation at BEP. The high resolution option was selected for modelling the nonlinear terms and the temporal term in the Navier-Stokes equations was solved using a second-order backward Euler scheme.

Both simulations were carried out using hexahedral mesh generated in ICEM 16.2 (Fig. 2). The mesh properties evaluated by CFX such as the minimum angle, the expansion factor and the aspect ratio are presented in Table 1.

The y^+ value was kept below 165 in the guide vane domain and 235 on the runner blade. In the draft tube domain y^+ was smaller than 5. Either standard or automatic wall functions (depending on the turbulence models) were used in all simulations.

The computational flow domain for the steady-state simulations included one guide vane passage, one runner blade passage and the full draft tube as shown in Fig. 3. The runner blade was scanned using a 3D optical scanning device (ATOS III system from GOM) and the geometry included the hub and tip clearances of the blade. The total number of cells for the Frozen Rotor and Stage simulations is 4.28×10^6.

Mulu *et al.* (2015) presented a mesh sensitivity analysis on the Porjus U9 draft tube mesh generated in ICEM. The runner mesh created in ICEM is coarser than the mesh employed by Mulu *et al.*(2015) due to the strict mesh quality criteria that are challenging to satisfy when using a scanned geometry. In order to perform a mesh sensitivity analysis on the runner and guide vane domains, a very fine mesh should be defined leading to a considerable increase in the mesh size along with the computational demands and the total simulation time.

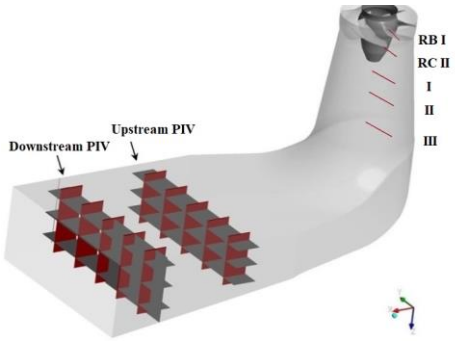

Fig. 1. Porjus U9 turbine model. LDA and PIV measurement locations.

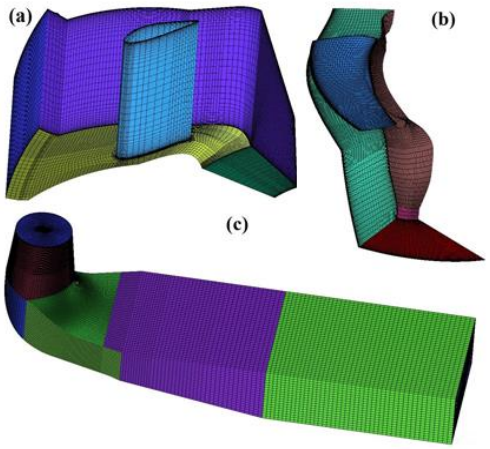

Fig. 2. Porjus U9 mesh. (a) guide vane. (b) runner blade. (c) draft tube.

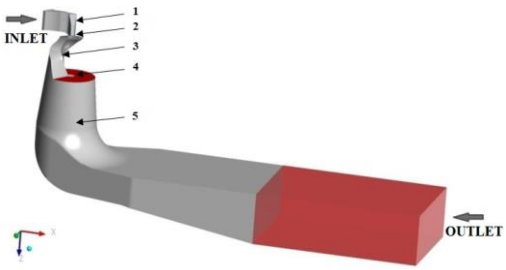

Fig. 3. Computational domains, steady-state simulations: 1. Guide vane domain. 2. Guide vane-Runner interface. 3. Runner domain. 4. Runner-Draft tube interface. 5. Draft tube domain.

The draft tube diffuser was extended with a 2 m straight channel. The outlet boundary condition was specified at the end of the channel. Considering the results from Mulu *et al.* (2011, 2015), the surface that separates the runner domain from the draft tube domain was lowered in order not to intersect the runner cone. The authors had mentioned in their study that the flow entering the draft tube was not accurately predicted because the Stage model calculates circumferential averages over strips of the interface. Since the Stage interface was just below the trailing edges of the blades, the hub and tip vortices were damped and flow separation occurred near the hub cone.

For the unsteady simulation, the guide vane domain was composed of 20 identical blades One guide vane was modelled and the mesh was rotated and copied. A similar transformation was performed for the 6 runner blades, (Fig. 4). The total number of cells for the entire model is 10.39×10^6. The time step was set to 4×10^{-4} s corresponding to 1.67° of the runner revolution. The simulation converged and a periodic pattern was noticed in the plots of the monitor points. The unsteady simulations were run for three full rotations after reaching convergence for each turbulence model.

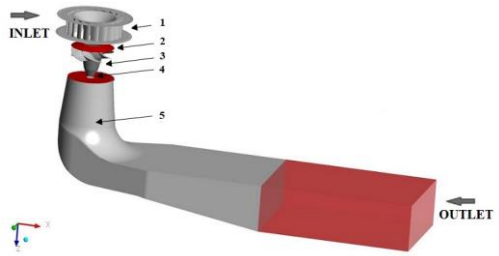

Fig. 4. Computational domains, unsteady simulations: 1. Guide vane domain. 2. Guide vane-Runner interface. 3. Runner domain. 4. Runner-Draft tube interface. 5. Draft tube domain.

At the inlet, the mass flow rate of 690 kg/s with a flow angle of 30° was imposed. A turbulence intensity of 5% was used, considering the investigations of Mulu *et al.* (2011) on the influence of the turbulence intensity. All walls were assumed smooth and a no-slip condition was specified. The outlet boundary condition was set as zero average static pressure.

Three different two-equation RANS turbulence models were used in the present work: k-epsilon, RNG k-epsilon and SST. The k-epsilon model is considered the standard industrial model. Using the scalable wall function, the model is robust and provides a good compromise between stability and accuracy. RNG k-epsilon is an improved alternative of the standard model that was developed to account for the effects of smaller scales of motion. This turbulence model includes an additional term in the ε equation for the interaction between turbulence dissipation and mean shear. RNG is expected to show improved prediction for high streamline curvature cases, such as hydraulic turbines. SST is a turbulence model based on the k-omega model that employs the automatic wall function. This model is using the k-epsilon turbulence model in the free shear flows and the k-omega turbulence model near the wall. SST is designed to produce accurate predictions of flow separation under adverse pressure gradients. Two more simulations were run for the curvature corrected SST model, using the standard value of 1 for the production correction coefficient C_{scale}, and a second value of 1.25. This correction improves the prediction of streamline curvature and system rotation by modifying the turbulence production, (Smirnov and Menter, 2009).

4. RESULTS AND DISCUSSIONS

The velocity profiles extracted from the CFD simulations, using different turbulence models are compared to the velocity profiles obtained experimentally (Amiri *et al.*, 2016a, Mulu and Cervantes, 2009; Mulu and Cervantes, 2011; Amiri *et al.*, 2016b).

Time averaged axial and tangential velocity profiles inside the runner blade channel and below the runner blades are analyzed for both the steady and unsteady simulations. Phase averaged results obtained from the unsteady simulations are also presented. For the LDA measurements in the draft tube cone (Mulu and Cervantes, 2009), comparisons are shown at section I just below the draft tube inlet (Fig. 1).

The velocity values are made dimensionless using the reference velocity calculated from the flow rate at BEP and the area at the corresponding section (i.e. RB I, RC II in the runner domain and section I in the upper part of the draft tube). All the radii are made dimensionless relative to the runner radius R = 0.25 m. Different methods are employed to obtain the average profiles. The LDA experimental values are averaged over several runner rotations at a fixed radial position. The profiles from the steady-state simulations are obtained by averaging over the conical plane equivalent to the LDA radial profile. The unsteady simulation results are provided by 21 monitor points defined along the LDA beams. The average is calculated over three runner rotations for each turbulence model.

In the draft tube diffuser velocity contours are compared against PIV measurement plots (Amiri *et al.*, 2016b). The velocity values are made dimensionless using the reference velocity obtained from the flow rate at BEP and the runner diameter D = 0.5 m.

The positive direction for the axial velocity is vertically downward, along the Z axis in the runner and draft tube cone (Fig. 3 and Fig. 4). In the draft tube diffuser, the axial positive direction is horizontal, along the X axis (Fig. 3 and Fig. 4).

4.1 Runner Domain

4.1.1 Steady-State Stage Simulations

The standard k-epsilon turbulence model, SST and

RNG k-epsilon are employed. The SST-CC turbulence model is also used and two values of the production multiplier C_{scale} are tested: C_{scale} = 1 and C_{scale} = 1.25. The first value is standard for the multiplier and the larger value corresponds to a strong concave curvature and enhanced turbulence production, according to Smirnov and Menter (2009). However, the two models show similar results therefore, only the results of the SST-CC using the default value are presented hereafter.

Figures 5 and 6 present the velocity profiles obtained from the steady-state Stage simulations at the runner domain in the blade channel (RB I, Fig. 5) and right below the blades at the runner cone (RC II, Fig. 6). The axial (V_{ax}^*) and tangential (V_{tan}^*) velocities at sections RB I and RC II are presented for the different turbulence models employed, together with the experimental values.

At the runner blade channel, (Fig. 5), the axial velocity is overestimated by 4% near the hub and shroud wall and 7% at the corresponding dimensionless radius of 0.7. The maximum overestimation occurs halfway between the hub and shroud at half the blade length. The SST models provide results only slightly closer to the experimental values. The tangential velocity is on the other hand underestimated by 20-24% all along the blade span. This behavior of RANS turbulence models is expected i.e. the tangential velocity provided by the guide vane-runner calculations is underestimated not only in steady-state simulations (Wilhelm *et al.*, 2016). However, the unsteady simulation will provide further insight.

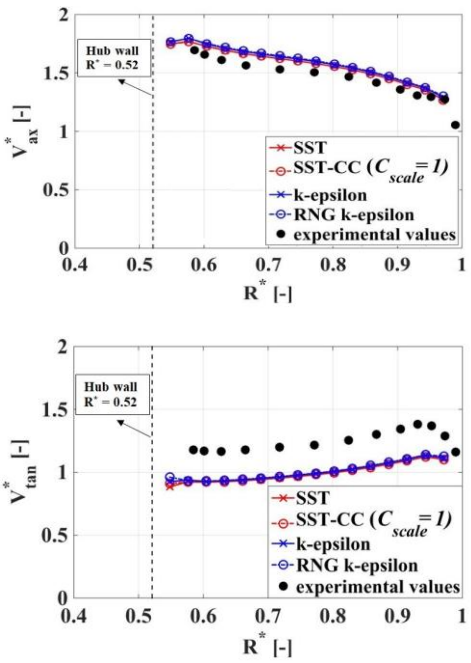

Fig. 5. Axial and tangential velocity profiles at section RB I, runner domain.

Below the blades, at section RC II, the simulated axial velocity values are more accurately predicted (Fig. 6). Slight discrepancies are shown near the shroud wall where the axial velocity is underestimated by less than 9%. Both hub and tip vortices formed in the blade clearances are captured by the simulations. The k-epsilon and RNG k-epsilon turbulence models show an overprediction of the hub jet whereas the SST and the SST-CC models, under predict the axial velocity. However, the differences are very small. The tangential velocity is also well captured showing that regardless of the upstream discrepancies, the runner provides a correct flow angle at the outlet. At the dimensionless radius R^* = 0.52, corresponding to the hub wall at the above section RB I, the tangential velocity is again underestimated.

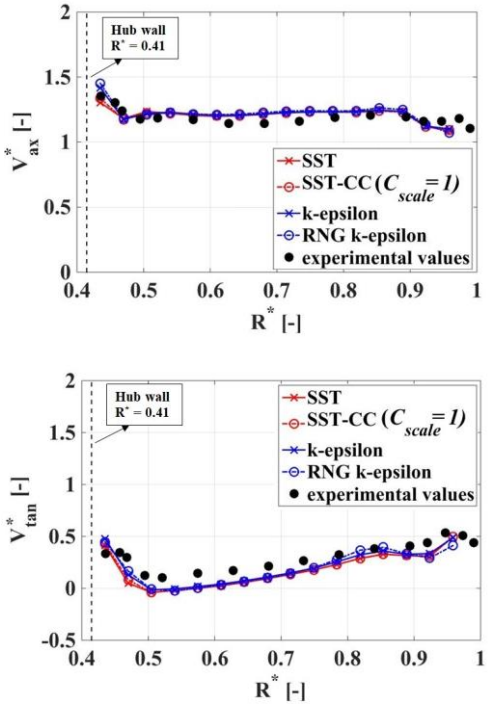

Fig. 6. Axial and tangential velocity profiles at section RC II, runner domain.

Figure 7 shows the turbulent kinetic energy values calculated from the experimental data compared to the values extracted from the steady-state simulations inside the runner and at the runner outlet. In order to calculate the velocity fluctuations v_{ax}' and v_{tan}' from the measurements, the phase average component of the signal was extracted from the original signal (Amiri *et al.*, 2016a). The kinetic energy was then computed as:

$$k = \frac{1}{2}\left(v_{ax}'v_{tan}'\right) \tag{1}$$

At the runner blade channel section all turbulence models show good agreement with the kinetic energy values determined experimentally. However, at the runner cone section, below the runner blades, considerable discrepancies between simulations and measurements are obtained near the hub. Here the kinetic energy is underestimated by all turbulence

models. This shows that the flow leaving the runner near the hub is not entirely captured by the simulations as it is also proven by the velocity profiles at the draft tube inlet presented in the following sections.

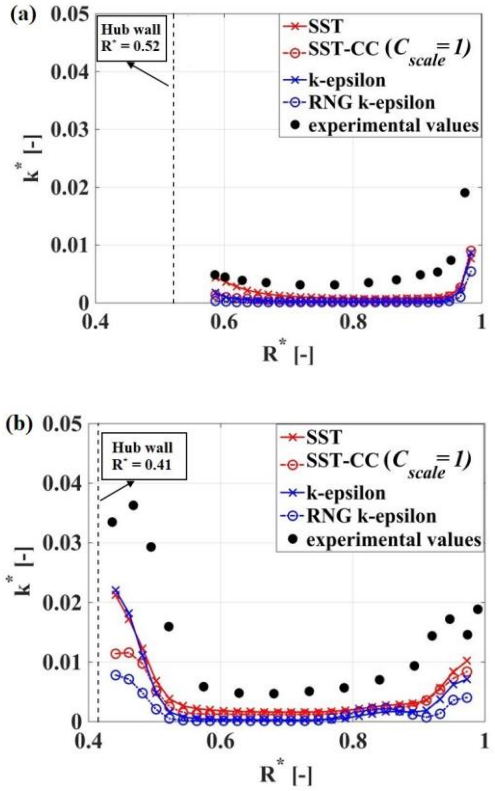

Fig. 7. Kinetic energy at sections RB I (a) and RC II (b), runner domain.

4.1.2 Unsteady Rotor-Stator Simulations

As previously presented, each unsteady simulation was performed for three runner rotations after convergence was achieved, i.e., a periodical pattern of the signals from the different monitor points. The velocity values are recorded by 21 monitor points defined along the LDA beam. Each monitor point provides a velocity profile $v'(x,t)$ that can be decomposed into three components: the time average $\bar{v}(x)$, periodic oscillations $\tilde{v}(x)$, and random fluctuations $v'(x,t)$. According to the Reynolds decomposition, the phase averaged profile is defined by:

$$\langle v(x,t)\rangle = \bar{v}(x) + \tilde{v}(x) = v(x,t) - v'(x,t) \tag{2}$$

An example of the phase averaged velocity over one runner revolution is presented in Fig. 8. Because the time step does not correspond to an integer number of degrees, the velocity values are not recorded at the exact same angular locations. Therefore the velocity values are not identical for all runner rotations.

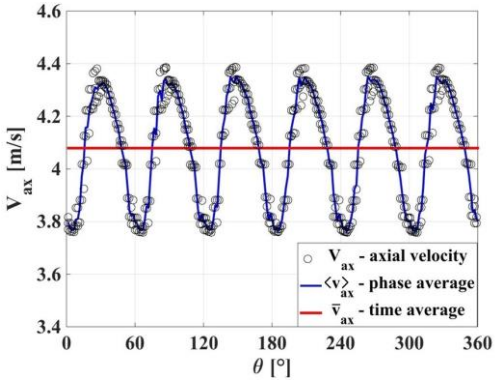

Fig. 8. Phase averaged velocity over one runner revolution, section RC II, R^* = 0.656.

Figures 9 and 10 present the time averaged velocity profiles obtained from the unsteady simulations. The results from the four turbulence models (k-epsilon, RNG k-epsilon, SST and SST-CC) are compared to experimental values. As opposed to the steady-state simulations, a distinction is now visible between the k-epsilon and the SST models. The main difference between the steady-state and unsteady simulations and the reason for this distinction are the interfaces. As stated in the description of the numerical case, the Stage interfaces are used to connect the guide vane, runner and draft tube domains in the steady simulations. At Stage interfaces, a circumferential average of the fluid flow variables is calculated. In the unsteady simulations, the interfaces are modelled using the Transient Rotor-Stator interface. The particles that cross such interfaces continue at the corresponding location, taking into consideration the time dependent relative position of the two domains.

At section RB I, Fig. 9, the axial velocity is accurately estimated. The largest differences are encountered near the shroud wall where the axial velocity is underestimated by 4.5%. The tangential velocity is best predicted by the k-epsilon models. Simulated values are 3% smaller in the hub region and identical to the experimental values near the shroud. Both SST models predict tangential velocities 9% lower than the measured velocities near the hub and 3% lower in the shroud region. However, the main justification for the SST results being slightly less accurate is the mesh refinement. As mentioned in the presentation of the numerical case, the y^+ values are larger in the runner domain near the blade-hub connection thus influencing the precision of the turbulence models.

The velocity profiles obtained from the unsteady numerical simulations at the runner cone, section RC II are similar to the profiles provided by the Stage simulations (Fig. 10). The shroud tip vortex is better captured in the axial velocity plot. Very small differences can be observed in the tangential velocity profile. The same underestimation of the tangential velocity at the dimensionless radius R^* = 0.52 is shown in the unsteady simulation results.

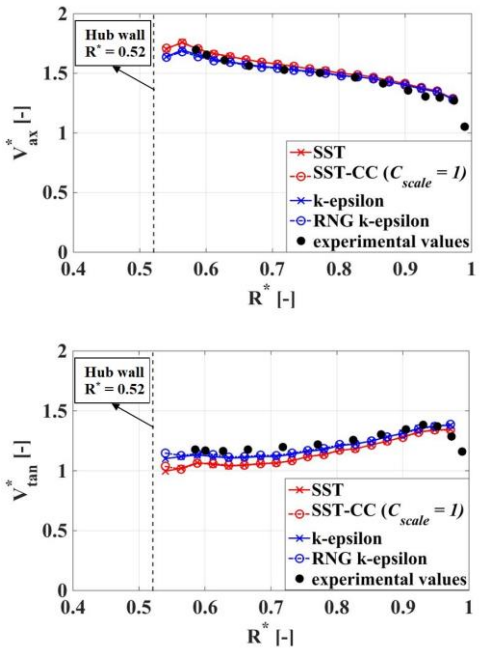

Fig. 9. Axial and tangential velocity profiles at section RB I, runner domain.

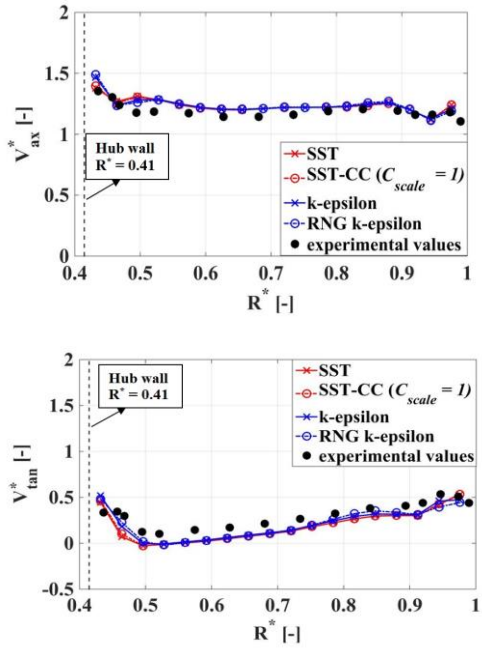

Fig. 10. Axial and tangential velocity profiles at section RC II, runner domain.

The contour plots of the phase averaged axial and tangential velocities are presented in Fig. 11 at the runner blade channel (RB I) and Fig. 12 below the blades (RC II). The numerically obtained values are compared to the experimental values. The results of two turbulence models have been selected, SST-CC and k-epsilon. All the contour plots are a top view of the flow and the runner rotates in the clockwise direction.

Both turbulence models show virtually the same velocity contours at section RB I (Fig. 11). The axial velocity component is larger near the suction side of the blades and decreases in the angular direction towards the pressure side of the next blade. Close to the blade tip, there is a low axial velocity region. The results validate the experimental hypothesis of Amiri *et al.* (2016a) that this effect is probably due to the tip clearance jet formed in the upper section of the blades. When the jet reaches the next blade, a secondary flow is formed and the axial velocity decreases. The tangential velocity is underestimated but the differences are smaller than in the steady-state simulation results. At section RB I the k-epsilon and RNG k-epsilon models capture smaller tangential velocities than the SST and SST-CC models, compared to the experimental values. Despite that, at section RC II below the runner blades, all turbulence models give comparable results. Similar to the steady-state simulation, it seems that the flow angle at the runner outlet is not influenced by the accuracy of the numerical predictions at the runner blade channels. All RANS models have difficulties in predicting flow structures such as secondary flows due to the assumption of isotropy in the eddy-viscosity model. As shown in the time average plots, the axial velocity is overestimated. The tangential velocity contour shows a lower tangential component near the blade pressure side. As the relative velocity is increasing along the blade, both turbulence models under predict the tangential velocity. The results confirm the fact that RANS turbulence models are not accurate near strong surface curvatures and in accelerated boundary layers (Alfonsi, 2009).

Figure 12 presents contour plots below the runner blades, section RC II. The velocity contours clearly capture the passage of the trailing edges of the runner blades for both the experiments and the simulations. The axial velocity decreases and at the same location, in the tangential velocity profile, there is an increase in the wake region. The hub vortices are captured by both turbulence models as six small areas of large axial velocity can be observed near the hub wall. Between two such areas, there is one low axial velocity spot as expected at the formation of vortices. The k-epsilon turbulence model overpredicts the axial velocity values near the hub and the spots are blurred out. The SST model on the other hand shows a better fit to the experimental values (Fig. 12c).

The numerically obtained phase averaged axial velocity results are in better agreement with the experiments.

The shroud tip vortices are better observed in the tangential velocity contours. The tangential velocity is underestimated near the hub wall. The k-epsilon model performs better but both turbulence models fail to capture the smooth variation of the tangential velocity in the radial direction. The low tangential velocity zone, which in the contours is shown as the dark blue area is larger in the simulations.

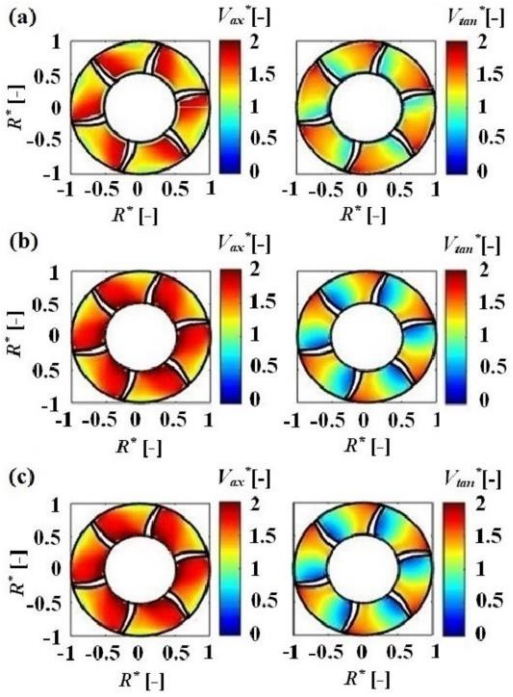

Fig. 11. Phase averaged axial (V_{ax}^*) and tangential (V_{tan}^*) velocity, section RB I. (a) Experimental values. (b) K-epsilon simulated values. (c) SST-CC simulated values.

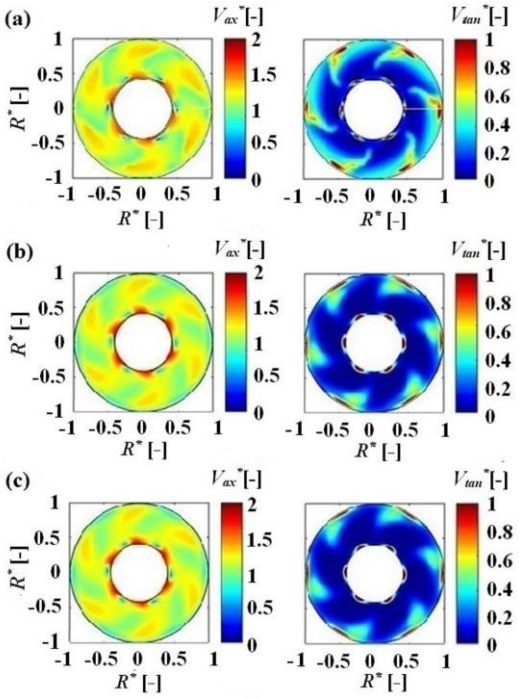

Fig. 12. Phase averaged axial (V_{ax}^*) and tangential (V_{tan}^*) velocity, section RC II. (a) Experimental values. (b) K-epsilon simulated values. (c) SST-CC simulated values.

4.2 Draft Tube Cone

4.2.1 Steady-State Stage Simulations

In the Stage numerical investigations of Mulu *et al* (2011), the flow in the U9 model draft tube was separated near the hub cone.

One potential reason was found to be the position of the runner-draft tube interface which was defined right below the trailing edges of the runner blades, approximately 60 mm below the runner centerline. As a consequence, the hub vortices were averaged at the draft tube inlet leading to flow separation.

In the present study, the runner-draft tube interface was lowered down to 300 mm below the runner centerline in order to investigate this aspect. There is no intersection between the runner hub and the interface and the flow is completely attached to the hub (Fig. 13).

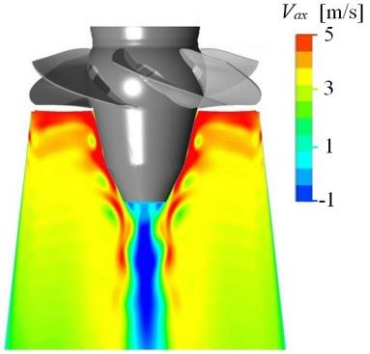

Fig. 13. Flow near the runner cone at mid plane.

Figure 14 presents the velocity profiles obtained from the steady-state Stage simulation at the draft tube domain, section I. Since this is the first section below the draft tube inlet, the center area contains the hub wake. The turbulence models behave similarly concerning the axial velocity. Differences are observed near the center of the draft tube where the SST model gives the best results. This behavior is expected since k-omega models such as SST are better in predicting flow recirculation (Alfonsi, 2009). However, the curvature corrected SST-CC model is not as accurate as the classical model at this section. In the tangential velocity profile, the overestimation near the center of the section is even more obvious. All turbulence models predict a tangential velocity higher by 20-23% than the measured values at the dimensionless radius R^* = 0.1÷0.15.

4.2.2 Unsteady Rotor-Stator Simulations

The unsteady simulations do not offer a considerable improvement of accuracy. Although they are more precise in capturing the flow in the area below the blades, the hub peak is again over estimated. However, this is most likely due to the clearance modelling. When approximating the surface of the blade over the scanned rough geometry, the clearance is decreased and therefore, the axial velocity is artificially increased. Figure 15 shows the time averaged velocity profiles obtained from the unsteady simulation at the draft tube domain, section I.

The axial velocity profile is best modelled by the k-

epsilon and SST turbulence models. As opposed to the Stage simulation, these two models do not provide different results as expected. Not the same can be observed for the tangential velocity profile. Here a clear improvement is provided by the SST model when compared to the k-epsilon or RNG k-epsilon models.

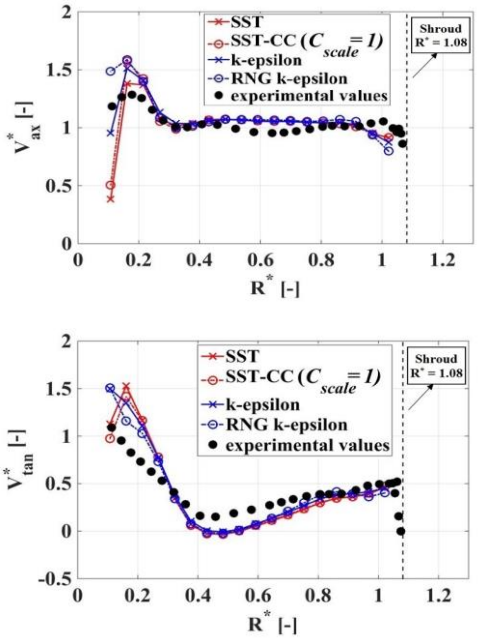

Fig. 14. Axial and tangential velocity profiles at section DT I, draft tube domain.

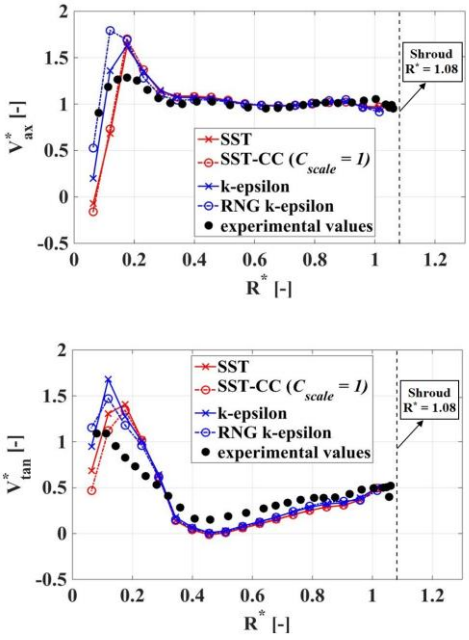

Fig. 15. Axial and tangential velocity profiles at section DT I, draft tube domain.

The phase averaged velocity contours at section I in the draft tube cone are presented in Fig. 16. The experimental values are compared to numerical results obtained for two turbulence models, SST-CC and k-epsilon.

The low axial velocity regions correspond to the blade wakes, overrepresented in the simulations compared to the experiments. The only difference between the two turbulence models can be seen below the runner cone. For both the tangential and the axial velocity contours, the SST-CC model predicts a larger area of recirculation in the center of the section.

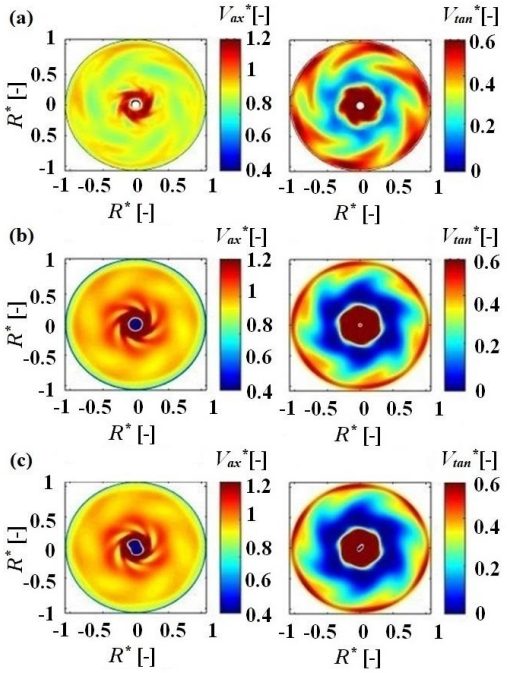

Fig. 16. Phase averaged axial (V_{ax}^*) and tangential (V_{tan}^*) velocity, section DT I. (a) Experimental values. (b) K-epsilon simulated values. (c) SST-CC simulated values.

4.3 Diffuser

The precision of the simulations decreases from the inlet of the model towards the outlet. Considerable differences in matter of accuracy were noticed between the first and the last section in the draft tube cone. In the straight diffuser, after the draft tube elbow, the numerical values differ even more from the experimental values.

Figure 17a shows the contour of the axial velocity inside the diffuser: obtained from the SST-CC unsteady simulation (left) and measured by Amiri *et al.* (2016b) (right). The simulated values are larger than the measured ones although the mass flow rate is the same. Despite the measurements showing the asymmetric flow, the simulation provides an almost symmetric flow after the draft tube elbow at the downstream section. Gubin *et al.* (1974) investigated the flow at the outlet of curved draft tubes and found that the asymmetry in the axial velocity profiles is directly influenced by the swirl leaving the runner, similarly to Amiri *et al.* (2016). In agreement with the conclusions of the aforementioned studies, the numerical simulations predict a weaker upstream swirl, confirmed also by

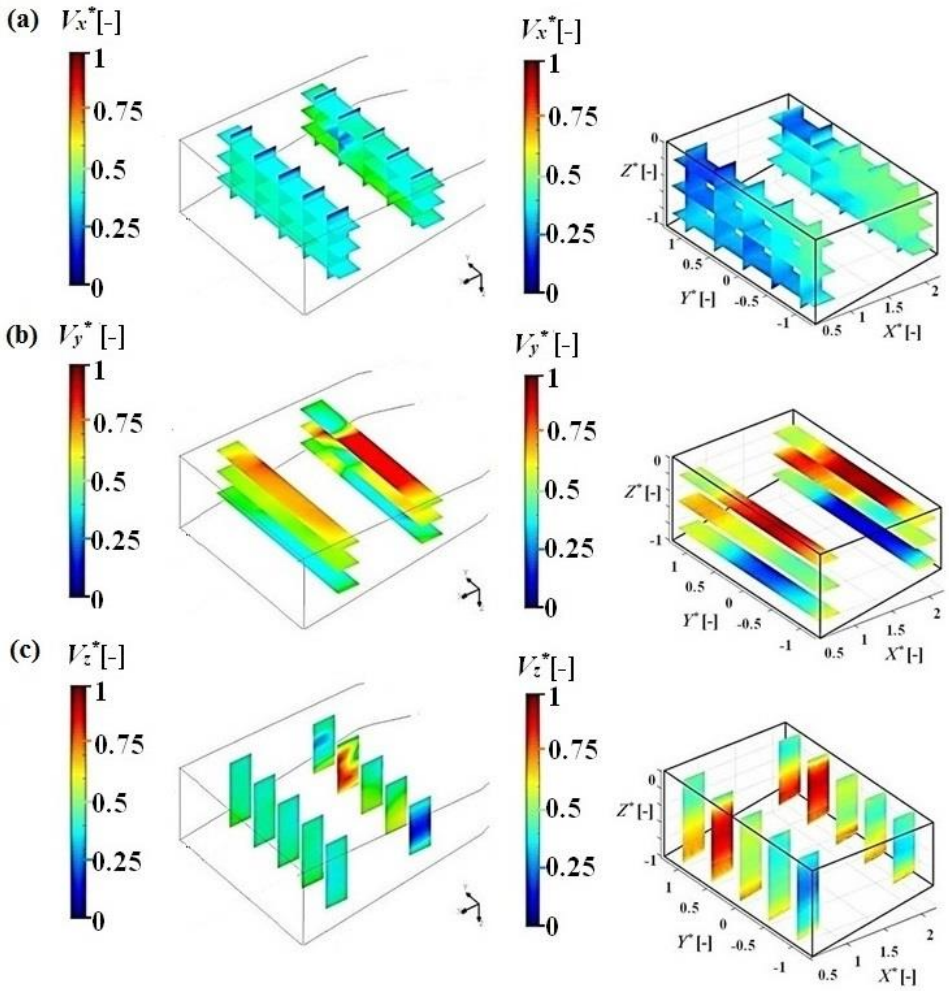

Fig. 17. Velocity contours in the draft tube diffuser (left) and PIV measurements (right): axial velocity (a) lateral velocity (b) and vertical velocity (c). Results of the SST-CC unsteady simulation.

the underestimation of the tangential velocity in the draft tube cone.

Figures 17b and 17c present the contours of the lateral and vertical velocities. These contours should give an image of the two vortices formed in the draft tube. This is clearly seen on the right side, where the measurements are presented. As estimated by Amiri *et al.* (2016b), 56% of the flow rate passes through the right half of the draft tube. The simulations show that only 53.7% of the mass flow rate passes through the right half. The lateral contour plots show a rather symmetric flow and the velocity values are larger than the experimental values in the upstream section and smaller in the downstream. In the simulation results, the vertical contour plots show the same nearly constant velocity field. As opposed to the measurements, very little recirculation is captured by the simulation.

5. CONCLUSION

Steady-state and unsteady simulations of the turbulent flow developed inside the Porjus U9 Kaplan turbine model at the BEP were performed. Three RANS turbulence models were employed: k-epsilon, RNG k-epsilon and SST. The computational domain included the guide vanes, runner and draft tube.

Numerical simulations were also carried out using the curvature corrected SST turbulence model, for two different values of the production correction coefficient C_{scale}. However, the two simulations showed very similar results.

Time averaged and phase averaged velocity profiles were compared to experimental data. The LDA measurements employed for the validation of the simulations were performed in the runner blade channel, below the runner blades and at the inlet of the draft tube cone. Further downstream, in the draft tube diffuser velocity contours were compared against PIV measurements. The numerical results proved to be insensitive to the turbulence model selection and reasonable agreement with the experimental data was achieved. The most accurate results were provided by the simulations using the k-epsilon and the SST-CC turbulence models but very small differences were obtained between the

different tested models.

Lowering the runner draft tube interface down to 300 mm below the runner centerline was a clear improvement of the numerical model. As a consequence, the flow was completely attached to the hub.

The velocity profiles in the runner showed the best fit to the experimental results whereas the largest deviations were found at the draft tube diffuser. Despite underestimating the tangential velocity at the runner blade channel section, the simulations provided accurate predictions of the flow at the runner cone section, just below the runner blades. The flow angle at the outlet of the runner was correct regardless of the upstream inaccuracy. Along the draft tube cone, an increasing difference between simulations and measurements was observed. Although the accuracy of the CFD simulations was good in the runner domain, towards the outlet of the turbine, precision decreased.

All turbulence models encountered difficulties when predicting the flow in the draft tube diffuser. The general discrepancies may be attributed to the over estimation of the energy losses leading to the underestimation of the tangential velocity and the weak upstream swirl captured by the numerical simulations.

ACKNOWLEDGEMENTS

The research presented was carried out as a part of "Swedish Hydropower Centre – SVC." SVC was established by the Swedish Energy Agency, Elforsk and Svenska Kraftnät together with the Luleå University of Technology, The Royal Institute of Technology, Chalmers University of Technology and Uppsala University (www.svc.nu).

REFERENCES

Abbas, A. and A. Kumar (2015). Development of draft tube in hydro-turbine: a review. *International Journal of Ambient Energy* 36.

Alfonsi, G. (2009). Reynolds-averaged Navier-Stokes equations for turbulence modelling. *Applied Mechanical Reviews* 62(4).

Amiri, K., B. Mulu and M. J. Cervantes (2016a). Experimental investigation of the interblade flow in a Kaplan runner at several operating points using Laser Doppler Anemometry. *Journal of Fluids Engineering* 138(2).

Amiri, K., B. Mulu, M. Raisee and M. J. Cervantes (2016b). Experimental study on flow asymmetry after the draft tube bend of a Kaplan turbine. *Advances and Applications in Fluid Mechanics* 19(2), 441-472.

Amiri, K., M. J. Cervantes and B. Mulu (2015). Experimental investigation of the hydraulic loads on the runner of a Kaplan turbine model and the corresponding prototype. *Journal of Hydraulic Research* 53(4), 452-465.

Arolla, S. and P. Durbin (2014). A rotation/ curvature correction for turbulence models for applied CFD. *Progress in Computational Fluid Dynamics an International Journal* 14(6), 341-351.

Belman-Flores, J. M., G. Camacho-Vazquez and A. P. Rodriguez-Munoz (2016). A review of hybrid systems including photovoltaic solar energy: General aspects in Mexico. *Journal of Renewable and Sustainable Energy* 84.

Cervantes, M. J. and F. Engström (2005). Eddy viscosity turbulence models and steady draft tube simulations. *Proceedings of the 3rd IAHR/ERCOFTAC, workshop on draft tube flow*, Porjus, Sweden.

Cervantes, M. J., U. Andersson and H. M. Lövgren (2010). Turbine-99 unsteady simulations – Validation. Paper presented at the *25th IAHR Symposium on Hydraulic Machinery and Systems*, Timisoara, Romania.

Elliott, K. J., E. Savory, C. Zhang, R. J. Martinuzzi and W. E. Lin (2012). Analysis of a curvature corrected model using a 90 degree curved geometry modelled after a centrifugal compressor impeller. 20st Annual Conference of the CFD Society of Canada.

Gubin, M. F., V. V. Volshanik and V. V. Kazennov (1974). Investigations of curved draft tubes with long exit cones. *Hydrotechnical Construction* 8(10), 949–956.

Hirth, L. (2016). The benefits of flexibility: The value of wind energy with hydropower. *Journal of Applied Energy* 181, 210–223.

Javadi, A., E. Krane and H. Nilsson (2015). Exploration of rotation/curvature correction method in hydropower application. Paper presented at the *8th International Symposium on Turbulence, Heat and Mass Transfer*, Sarajevo, Bosnia and Herzegovina.

Keck, H. and M. Sick, (2008). Thirty years of numerical flow simulation in hydraulic turbomachines. *Acta Mechanica* 201, 211–229.

Lipej, A. and C. Poloni (2000). Design of Kaplan runner using multiobjective genetic algorithm. *Journal of Hydraulic Research* 38(1), 73-79.

Mulu, B. and M. J. Cervantes (2009). Experimental investigation of a Kaplan model with LDA. *Proceedings of the 33rd Congress of IAHR*, Vancouver, Canada.

Mulu, B. and M. J. Cervantes (2011). Phase-resolved velocity measurements in a Kaplan draft tube model. *Proceedings of the 4th IAHR International Meeting on Cavitation and Dynamic Problems in Hydraulic Machinery and Systems*, Belgrade, Serbia.

Mulu, B., M. J. Cervantes, T. Vu, C. Devals and F. Guibault (2011). Effects of inlet boundary conditions on Kaplan draft tube simulation

accuracy. Paper presented at *HYDRO 2011 Conference*, Prague, Czech Republic.

Mulu, B., M. J. Cervantes, T. Vu, C. Devals and F. Guibault (2015). Simulation-based investigation of unsteady flow in near-hub region of a Kaplan turbine with experimental comparison. *Engineering Applications of Computational Fluid Mechanics* 9(1), 139-156.

Prasad, V. (2012). Numerical simulation for flow characteristics of axial flow hydraulic turbine runner. *Energy Procedia* 14, 2060-2065.

Rahi, O.P. and A.K. Chandel (2015). Refurbishment and uprating of hydro power plants - A literature review. *Renewable and Sustainable Energy Reviews* 48, 726–737.

Roussopoulos, K. and P. A. Monkewitz (2000). Measurements of Tip Vortex Characteristics and the Effect of an Anti-Cavitation Lip on a Model Kaplan Turbine Blade. *Flow, Turbulence and Combustion* 64, 119-144.

Smirnov, P. and F. Menter (2009). Sensitization of the SST turbulence model to rotation and curvature by applying the Spalart-Shur correction term. *Journal of Turbomachinery* 131.

Spalart, P. R. and M. L. Shur (1997). On the sensitization of turbulence models to rotation and curvature. *Aerospace Science and Technology* 1(5), 297-302.

Trivedi, C., M. J. Cervantes and O. G. Dahlhaug (2016a). Experimental and Numerical Studies of a High-Head Francis Turbine: A Review of the Francis-99 Test Case. *Energies* 9(2), 74.

Trivedi, C., M. J. Cervantes and O. G. Dahlhaug (2016b). Numerical Techniques Applied to Hydraulic Turbines: a Perspective Review. *Applied Mechanics Reviews* 68(1).

Wilhelm, S., G. Balarac, O. Metais and C. Segoufin (2016). Analysis of Head Losses in a Turbine Draft Tube by Means of 3D Unsteady Simulations. *Flow Turbulence and Combustion* 97, 1255–1280.

Wu, J., K. Shimmei, K. Tani, K. Niikura and J. Sato (2006). CFD-Based Design Optimization for Hydro Turbines. *Journal of Fluids Engineering*, 129(2).

Vu, T. C., M. Gauthier, B. Nennemann, H. Wallimann and C. Deschênes (2014). CFD analysis of a bulb turbine and validation with measurements from the BulbT project. Paper presented at *the 27th IAHR Symposium on Hydraulic Machinery and Systems*, Montreal, Canada.